AIAA 97–3169
A Performance Evaluation of MEMS-based Micronozzles

R.L. Bayt, A.A. Ayon, and K.S. Breuer
Department of Aeronautics and Astronautics
Massachusetts Institute of Technology
Cambridge, MA 02139

33rd AIAA/ASME/SAE/ASEE Joint Propulsion Conference & Exhibit
July 7-9, 1997/ Seattle, WA

For permission to copy or republish, contact the American Institute of Aeronautics and Astronautics
1801 Alexander Bell Drive, Suite 500, Reston, VA 22091

A Performance Evaluation of MEMS-based Micronozzles

R. L. Bayt[†], A. A. Ayon[E], and K. S. Breuer[*]
MIT Fluid Dynamic Research Laboratory, Rm. 37-401, 77 Massachusetts Ave., Cambridge, MA 02139

Abstract

An investigation is made into the modeling, design and testing of micron scale Laval nozzles. Such nozzles can provide orbital maneuvering for small spacecraft or attitude control and stationkeeping for their larger counterparts. The flow in the nozzle is modeled by means of a two dimensional finite volume Navier-Stokes simulation which predicts viscous losses with a decrease in nozzle scale. Calculations show mass flow is reduced to 93% of the ideal inviscid flow for a throat Reynolds number of 500. The nozzles modeled are fabricated through deep reactive ion etching in an inductively coupled plasma. Nozzle throat dimensions of 30 microns reduce to 20 microns over the depth of the nozzle. Nozzle testing reveals choked conditions exist, and the flow rates are similar for different geometries of the same throat dimensions.

Introduction

The current trend in space system design is to reduce program life cycle cost through reduced complexity of satellite missions. This has been done by limiting mission scope, and in turn reducing the mass of spacecraft. A great asset in this pursuit will come from the use of Microelectromechanical Systems (MEMS), an offspring of the microelectronics revolution. The trend toward small spacecraft will only be possible with the miniaturization of spacecraft systems, and this in turn will be realized with demonstrated microcomponents.

This work focuses on the development of micropropulsion systems. Currently, large satellites use low thrust (~0.1 N) devices for stationkeeping and attitude control when slew rate is not critical. With the reduction in scale predicted for the next generation of satellite systems, these same tasks can be accomplished by propulsion systems on the order of 0.1-10 mN [1] for spacecraft on the order of 1-50 kg. As technology drives the total mass less than 10 kg, these micropropulsion systems can also be used for orbit transfer and rephasing. But, the role of these systems will ultimately be limited by the performance they can deliver.

This paper focuses on performance issues associated with MEMS cold gas systems. This work will lay the foundation upon which more advanced systems such as resistojet and arcject technologies will rest. Even the cold gas system will play a role critical in some mission designs. Sutton [2] described propulsion architectures which are dominant for given mission requirements (notably I_{sp} vs. thrust requirements). London [3] expanded this analysis to examine new technologies and their applicability at small scales. This work is summarized in Figure 1. As seen here, cold gas thrusters are of importance in some mission scenarios. And, with the performance enhancement afforded through resistive heating or arc-discharge, this realm will grow considerably.

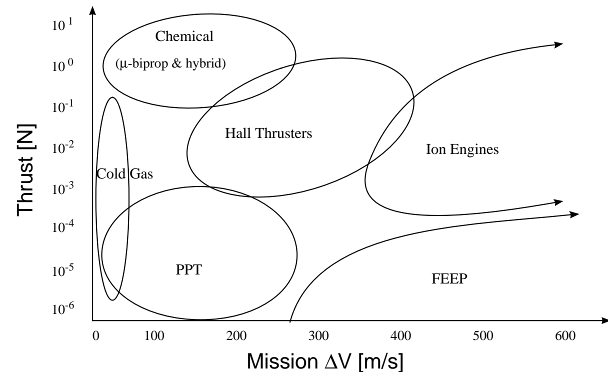

Figure 1: Domains of applicability for propulsion technologies [3]

Advantages of Micropropulsion

The primary driver for moving to smaller spacecraft had been the reduction of launch costs. However, this benefit lessens because at the minimum, at least one launch vehicle is still required, and the complexity of integrating more than three or four payloads becomes prohibitive. Therefore, there must be performance related drivers for moving to smaller systems. The primary advantage comes from the "cubed-squared" law which states that as scale is reduced properties which are a function of the volume (mass)

[†] Research Assistant, Student Member AIAA
[E] Post-Doctoral Research Associate, Microsystem Technology Lab
[*] Associate Professor, Senior Member AIAA

Copyright © 1997 by the Massachusetts Institute of Technology. Published by the American Institute of Aeronautics and Astronautics, Inc. with permission.

will decrease faster than those which are a function of area (thrust). For example, if a nozzle is modeled as a pressure vessel for which the mass can be approximated as the area multiplied by the wall thickness and density, the thrust-to-mass ratio is

$$\frac{F}{m} \propto \frac{P_c\ A_t\ C_f}{P_c\ SA\ L} \propto \frac{L^2 C_f}{L^3} = \frac{C_f}{L} \qquad (1)$$

where P_c is the chamber pressure, A_t is the throat area, SA is the nozzle surface area, C_f is the coefficient of thrust, and L is the characteristic length. The thrust-to-mass ratio of a simple nozzle, therefore, increases as scale is reduced. Scaling laws applied to other components suggest that the total performance-to-mass ratio of a blowdown propulsion system without combustion will increase. [3]

The previous example focused on advantages afforded to a simple reduction in scale. However, if this reduction is achieved through the use of micromachining technology, additional advantages become apparent. Drawing upon the wealth of experience in the microelectronics industry, components etched into silicon can be produced in quantities numbering from hundreds to thousands of devices per wafer. This batch processing can lead to mass production of separate devices, or redundancy built directly into a microsystem chip. This also allows any required electronics to be machined on the chip with the device, eliminating the need for subsystem integration and interface testing.

In addition, since the workhorse material of the industry is silicon, micropropulsion components enjoy the advantage of working with a single crystal material. This offers high strength-to-weight ratio, a fairly high thermal conductivity and a melting temperature (1700 K) high enough for some resistojet applications. With the advent of micro-machined refractory materials such as silicon carbide, the options for future propulsion systems greatly increase.

Micropropulsion Issues

There are several challenges to working with MEMS-based propulsion systems. The first is the inherent loss due to viscous forces acting on fluid elements at this small scale. In addition, the performance of these systems are intimately connected with the means by which they are fabricated. Currently only 2-D extruded features are possible with the anisotropic etching techniques presented here, and the variation of feature geometry with depth will impact performance. However, a 2-D nozzle does not have the flow divergence loss in the direction normal to the nozzle plane; whereas, axisymmetric nozzles have flow divergence in all directions.

Historical Effort

Nozzle performance at small scale has been studied on a number of occasions. Most notably, it was begun with Rothe's E-beam measurements of flows in a nozzle with a 5 mm throat [4]. With the revived interest in resistojets in the mid-80's for Space Station re-boost applications, as well as satellite station keeping, the micropropulsion initiative was begun. Grisnik et al. [5] investigated nozzles with throat diameters on the order of 650 microns. Each of these test cases were machined through conventional methods and are orders of magnitude larger than what is available through MEMS. In order to reduce the thrust and hence minimize the impulse bit, these nozzles were run at low chamber pressures which results in low Reynolds numbers and hence lower I_{sp}.

In 1996, Janson et al. [6] presented results for batch fabricated micronozzles which can achieve the same low thrust as their conventionally machined counter parts, but at a higher I_{sp} because their smaller throat area allows a higher chamber pressure while maintaining low thrust. Janson's nozzle geometries were limited to converging-diverging orifices manufactured by anisotropic etching along crystalline planes and laser milling. The minimum throat diameter tested in this program was 200 microns for a 2.5:1 expansion ratio circular orifice.

This work investigates the performance of micronozzles manufactured through deep reactive ion etching (DRIE) with an inductively coupled plasma. The procedure described herein will demonstrate a reduction in scale from previous nozzles by an order of magnitude while maintaining a smoothly contoured geometry for maximum performance.

Numerical Modeling

Background

Viscous supersonic flow was first studied in pipes with friction in what is commonly known as the Fanno formulation. Williams [7] first applied a slender channel approximation to the Navier-Stokes equations which allowed an application to supersonic nozzle flow. This formulation was used by Rae [8] to provide an analytical model for Rothe's work. Rae found that for small divergence angles at low Reynolds numbers the viscous boundary layer fills the nozzle and there is a shockless transition to subsonic flow. This is accomplished by a thermalization of the flow energy. Temperature profiles reveal that the kinetic energy of the fluid is converted into heat energy which is convected out the exit.

Aside from this result, the best models have come from numerical simulations. These range from inviscid method of characteristics models with boundary layer corrections such as the Rao code for nozzle design to full Navier-Stokes simulations. Kim [9] developed a finite volume code which was used to determine trends in performance with a variation in geometry. He identified the trade-off between viscous losses due to merging boundary layers and the divergence losses due to the radial component of thrust nulling with its symmetric counterpart. His code found that for nozzle flows with a throat Reynolds number less than 1150 the 30-degree half-angle conical nozzle outperformed the 20-degree and the bell nozzle both of which improves the directed thrust for the same area-ratio.

However, as the scale is reduced not only is the Reynolds number lowered, but the characteristic length nears the mean free path of the fluid. This condition results in velocity slip at the wall, a feature not modeled by Kim. However, this can be taken into account using direct simulation methods as done by Zelesnik et al. [10]. They model the geometries of the Grisnik experiments but with a DSMC code. While a more tangible result, the computational effort was enormous.

Numerical Method

With the foresight of this previous work, a computational model is developed which best suits a prototype design and test program. Prior to fabrication and testing, a baseline nozzle is established to benchmark performance. This baseline is modeled using a finite volume approximation of the Navier-Stokes equations in two dimensions. Due to the nature of the problem, flow through a high aspect ratio extruded nozzle, a two-dimensional model should adequately simulate the core viscous nozzle flow. A first order calculation predicts a sidewall boundary layer of the same order as those found on the curved nozzle surfaces in the simulation. This value is approximately 20 microns at the exit of the nozzle for the baseline case. For a 500 micron deep etch, the core flow is more than 90% of the flow, justifying a 2-D model. The model employs Jameson time-stepping with fourth order artificial viscosity to maintain stability. Sutherland's law is used to model the temperature dependence of viscosity.

The governing equations are non-dimensionalized by the throat conditions, and Reynolds number is calculated as

$$\mathrm{Re} = \frac{\rho^* a^* D^*}{\mu^*} = \frac{\dot{m}}{\mu^*} \qquad (2)$$

where ρ^* is density, a^* is speed of sound D^* is throat width, and μ^* is viscosity, all at the throat condition.

Boundary Conditions

The inlet conditions are set by the test case inlet total pressure. The nozzle inlet is considered to have no transverse or radial velocity component and the inlet conditions are set by the characteristic boundary conditions derived from plenum total pressure. To improve stability in the solution a small section of straight channel was introduced at the entrance of the nozzle. This set the inlet Mach number equal to that found from the subsonic branch of the isentropic relations for flow through a converging-diverging nozzle. This prevents a discontinuity between the assumed zero velocity in the chamber and a finite entrance Mach number.

The exit conditions consist of two regions, the supersonic core flow, and the subsonic boundary layer. The core flow is extrapolated from the interior to the exit conditions. The subsonic boundary layer flow should be affected by the exit pressure, but in general, experiments have shown that unless the back pressure is high enough to cause separation, the effect is negligible. Therefore, the extrapolation techniques are applied throughout the exit plane. This can be likened to the boundary layer assumption reducing the Navier-Stokes equations to parabolic equations. A similar technique was used by Kim [9] and proved to be acceptable.

The wall conditions are modeled as isothermal with velocity slip. The isothermal condition is justified because the thermal mass of silicon is much higher than that of the gas, in addition to silicon having a relatively high thermal conductivity. Velocity slip is imposed by

the Maxwell [11] formulation, where wall velocity is defined by

$$\frac{u_w}{a} = \frac{2-F}{F} Kn \frac{du^*}{dy^*} \tag{3}$$

where F is the wall accommodation coefficient, Kn is the local Knudsen number, and a is the throat speed of sound. u^* and y^* are also normalized by throat conditions. The local conditions are computed at each step and the wall slip is modified based on the local velocity gradient and pressure. The accommodation coefficient is a function of the fluid and wall properties. Studies by Arkilic [12] suggest F=0.8 for a prime silicon with native oxide interacting with an N_2 flow. In this model, F is 1.0.

In addition, a zero pressure gradient condition is imposed at the walls. The pressure gradient is computed from an energy balance at the wall as

$$\left.\frac{\partial P}{\partial n}\right|_w = \frac{\rho_w V_w^{\ 2}}{R_w} \tag{4}$$

In this equation, ρ is the density, V is the wall velocity, and R is the wall radius of curvature. The right hand side of this equation is approximately zero because the velocity slip is nearly zero where the wall has curvature. The velocity slip is important only in flat regions (infinite radius of curvature) of a conical nozzle, which allows the right hand side of equation (4) to be approximately zero. Therefore, this constant pressure at the wall condition allows temperature velocity and density to all be specified. This assumption breaks down for models with wall curvature in low density regions; however, the impact of wall slip on total performance is minimal.

Nozzle Geometry

To provide a basis of comparison to other low thrust nozzles, geometries similar to those studied by Grisnik [5], Kim [9], and Zelesnik [10] were chosen. The geometries were all variations on the conical, bell and trumpet nozzles. The geometries were designed using traditional nozzle design criteria for throat radius and inlet diameter. Area ratios were chosen that would give high Mach numbers at the exit and would provide adequate expansion to investigate the merging of boundary layers and possible thermalization of flow energies. At the same time, exit area ratios were kept low enough to avoid the need for high vacuums to prevent flow separation, in these initial studies.

Each of these were modeled with structured grids on the order of 100x100, with grid point clustering near the walls. This mesh size was selected after computational tests determined grid independence of the solution. The Reynolds numbers examined ranged from 200-10000. Some sample results of a 4.2:1 area ratio conical nozzle flow are shown in Figure 2 through Figure 4. This case was chosen for illustration due to the ease of visually discerning all points of the flow. The nozzles fabricated and tested are at much larger area ratios. Figure 2 depicts the variation in Mach number along the length of the nozzle. The curved nature of the Mach lines is revealed through the model. The sonic condition exists downstream of the geometric throat. This figure also illustrates the thickness of the boundary layer. The subsonic boundary layer is 2% of the exit area. The boundary layer for which the edge velocity is less than 99% of the core flow fills 21% of the nozzle. Figure 3 shows how the Knudsen number varies, and velocity slip become important near the exit of the nozzle. However, case studies show that the velocity slip has very little effect on the final performance of the nozzle. Figure 4 illustrates the variation of coefficient of discharge with Reynolds number, as well as I_{sp} efficiency. These results are encouraging since high values of C_d and subsequently I_{sp} can be achieved at these small scales. Model comparisons with test data are described in the section on testing.

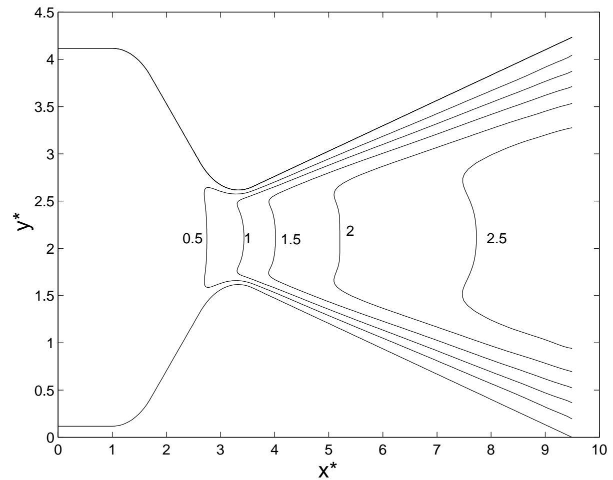

Figure 2: Mach contours in a 4.2:1 area ratio conical nozzle Re = 1000 exhausting to vacuum (note the scales are expanded for readability)

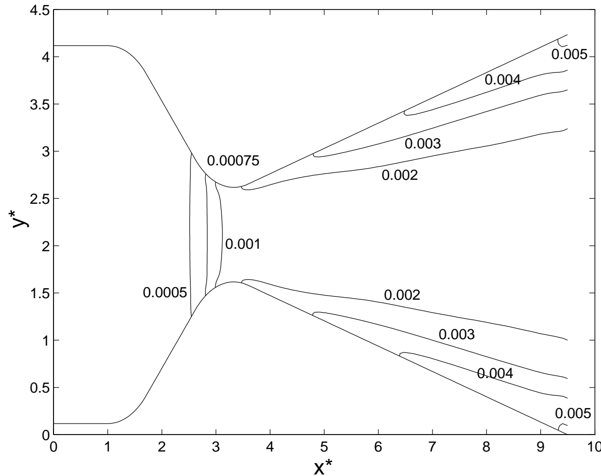

Figure 3: Knudsen Number contours at Re = 1000 exhausting to vacuum

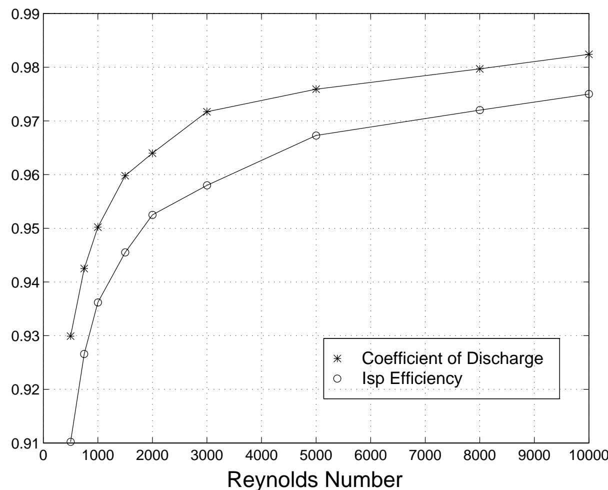

Figure 4: Performance Variation of the 4.2:1 area ratio nozzle with Reynolds Number

Fabrication of Micronozzles

The Process

Etching technology has been used for many years in integrated circuit production. With a wet chemical etch it is possible to pattern trenches with depths up to hundreds of microns. The drawback is the isotropic nature of the etch. Isotropic etching has an etch rate equal in all directions. This results in patterns which have curved wall and hence variable cross-sections. With the development of reactive ion etching, a plasma bombardment etch, directed ions are used to maintain anisotropy during the etching process. The high temperature and relatively high density plasma is directed at a silicon wafer which is protected by an organic polymer photoresist patterned through photolithography. The ions are accelerated through a potential difference between the glow discharge and the platen that the wafer rests upon. The exposed areas of the silicon react with the chemical species and the by-products diffuse into the plasma.

The degree of anisotropy previously available allowed features of aspect ratios on the order of 15 to 1 to be produced [13]. At the heart of this research program is a new device produced by Surface Technology Systems called the Multiplex ICP [14]. This etcher is based upon an inductively coupled plasma (ICP) which accelerates the ions with a tight control on directionality. The anisotropy is achieved by alternating between an etchant gas flow (SF_6) and a passivation step. After a specified etch time, which has been previously set, C_4F_8 is used to coat the exposed areas, and passivate the surface. Upon returning to the etchant flow, the exposed areas normal to the flow are quickly cleared of the C_4F_8 coating, but the walls remain resistant to the indirect exposure to the etchant. In addition, a coil radiates energy to the plasma increasing the density. Aspect ratios have been achieved as high as 40 to 1. With this capability, it is possible to fabricate nearly two dimensional flow channels, and the end-wall effects on the core flow are minimal.

The STS etcher is capable of etching through a silicon wafer (nominal thickness 500 microns) with 10 microns of variation in the feature geometry. There are several variables which affect the performance of the etch, and ultimately control the etch profile and etch rate. These variables are SF_6 flowrate, C_4F_8 flowrate, cycle time for each step, overlap time between steps, power to the coil, power to the platen, and chamber pressure.

The fabrication process is tuned by determining what is the appropriate recipe for the pattern being etched. In addition to the etcher inputs, the profiles vary with exposed area, feature size, and the ratio of the size of features near each other. One of the most difficult hurdles to overcome is the loading effect, or the differential etch rate found between large and small features. Due to this, features have variations in cross-section, as well as sloping floors in the flow cavity.

Once a suitable recipe is determined, and an etch results in a flow cavity profile that is nearly two dimensional, the nozzle is capped on the upper and lower surface by glass plates. These plates are anodically bonded to the silicon surface which results in a seal with yield strengths reported as high as 10 MPa [15], which is higher than the fracture limit of the glass. The anodic bond, performed by an Electronic Visions Aligner/Bonder, is formed by heating the glass and silicon to 500°C and applying a 800 V potential difference between the plates, and 2400 mbars of pressure. Mobile positive ions in the glass migrate

away from the silicon toward a cathode creating a permanent space charge which persists after the Silicon-Glass wafer is cooled and the voltage removed. The glass used in this experiment is 7740 Pyrex and has been pre-drilled ultrasonically to allow gasses to be introduced via 0.040" tubing into the settling chamber as well as a port to evacuate the chamber at the exit.

Sample Results

Figure 5 shows a scanning electron micrograph of the micronozzle and chamber design. The octagon at the entrance to the nozzle is the settling chamber. This is pressurized to create flow through the nozzle, and the nozzle empties into the square feature, which is maintained at vacuum levels. This feature is then capped by two glass plates to create a flow channel. For thrust tests, the square will be diced through such that the flow discharges from the system resulting in a net thrust.

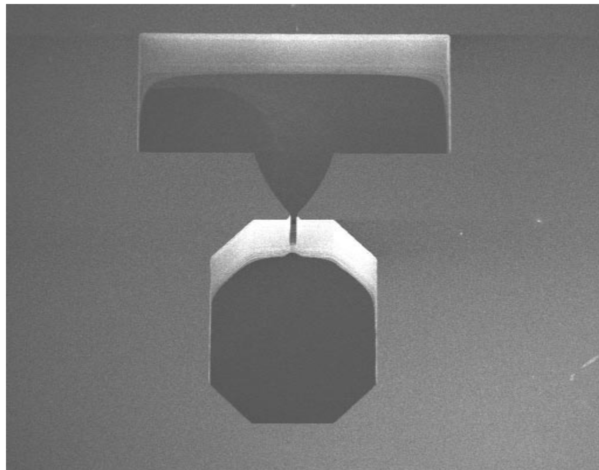

Figure 5: System view of a bell Micronozzle, Settling Chamber, and Vacuum Chamber. Nozzle throat is 31 microns and the area ratio is 25:1.

Figure 6 is an enlargement of the throat region. In this picture it is apparent that there is some loading effect which is evident in the pinching of the throat region. This is due to such a small feature being located next to the large feature of the tank. The etch rates in this region are so different, that the nozzle does not fully develop by the time the etch is completed. This is also apparent near the bottom of the cavity, where the inlet nozzle geometry begins to distort, and is actually larger than the area above it. This is also a characteristic of the loading effect. However, as mentioned in Kim [9], as long as the inlet is smoothly varying, its geometry will have little affect on performance. This has been corroborated by test cases run in the numerical model.

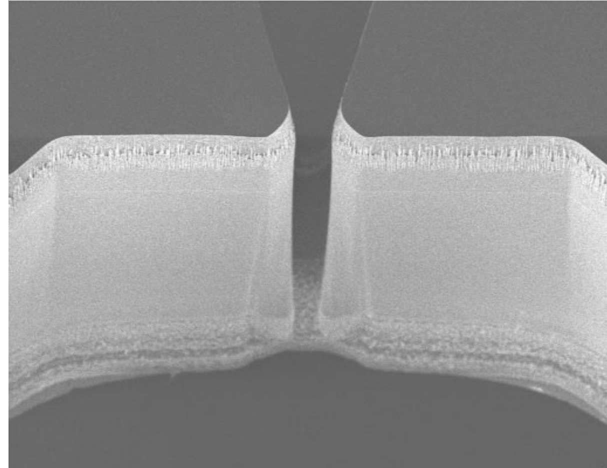

Figure 6: SEM of inlet and throat region of nozzle

Figure 7 shows the expansion region of a bell nozzle. At the exit plane, there is a slight variation in cross-section. However, with the variation localized at the exit plane, effects on performance should be minimal, as the flow at this point is experiencing its maximum expansion.

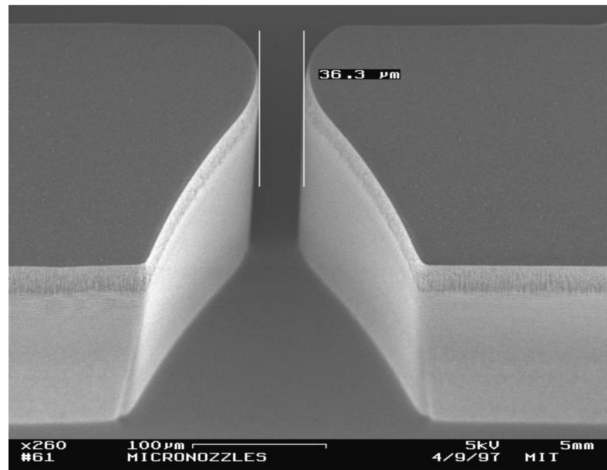

Figure 7: Bell Nozzle Expansion Region

Finally, wall roughness may be a major factor in nozzle performance. In the supersonic portion of the nozzle, any significant wall variation causing a flow perturbation may result in a shock, which may cause a pressure rise in the flow and reduce the thrust and I_{sp} of the nozzle. A characteristic of the STS etcher is a band of surface roughness concentrated near the top of the

wafer. This can be attributed to being near the plasma during the etch and receiving a larger number of impacts than the portion of the walls deeper in the trench. Also, when the photoresist is developed, it slopes from maximum thickness to zero thickness at the feature edge. As the etch proceeds, the photoresist in the region near the feature will breakdown early because it is thinner. This results in the slight taper near the top surface. This roughness band is limited to the top 20 microns of the channel. Below this however, the wall surface roughness variation is less than 1.5%, or about 300 nm.

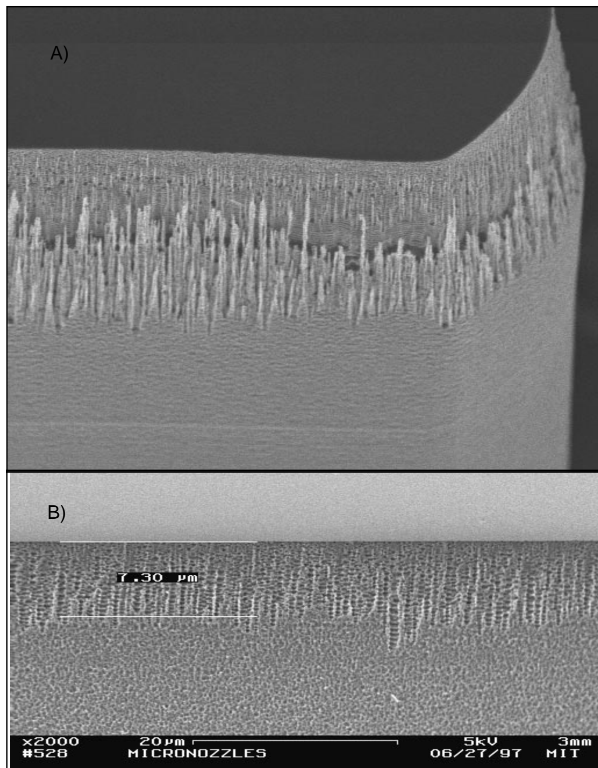

Figure 8: Roughness band A) 20 microns wide at the top of the flow channel with a photoresist mask B) 7.0 microns with an oxide mask reinforcing the photoresist.

To prevent premature breakdown of the photoresist, a 0.25 micron layer of silicon dioxide was grown on the surface of the wafer. This was coated and patterned with resist. A buffered oxide etch was performed which cleared the pattern of oxide. The oxide reinforced the photoresist to prevent this breakdown and scoring. As seen in Figure 8, the band is reduced to approximately 7 microns and the roughness remains submicron.

Nozzle Testing

A testing program was designed to demonstrate a working system, which overcomes one of the fundamental challenges of MEMS, packaging. Packaging is the interface of microdevices with the macroscopic world. In addition, since flow in microchannels suffer from high viscous losses, the mass flow rate for a variety of nozzle geometries at different feed pressures is to be evaluated.

The test set-up utilizes grade 5.0 nitrogen regulated to chamber pressures ranging from 1 to 150 psia. A 0.5 micron filter is in the line to prevent contamination from entering the nozzle. The gas is run through 1/8" copper tubing into a manifold on which a Honeywell Microswitch AWM 43300 flow meter is mounted. The exit of the manifold runs into Scanivalve fittings mated to 0.063" nylon tubing. The tubing is then reduced through a final fitting to a 0.040" stainless steel tube which is epoxied into the feed holes drilled into the glass. The vacuum system is of similar design and is epoxied to the exit chamber of the nozzle. A pressure transducer is located 10 cm upstream of the nozzle inlet.

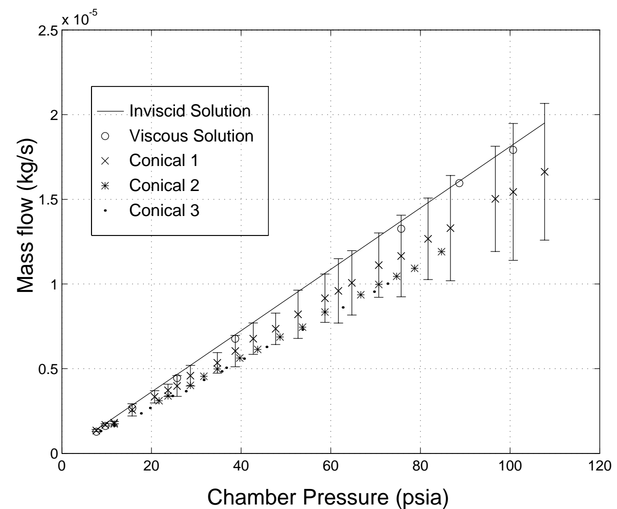

Figure 9: Flow rate dependence on pressure drop across a 6.5:1 area ratio conical nozzle (Throat Diameter =31 microns)

Figure 9 depicts flow measurements made with a variation in plenum pressure. Each of these tests were performed on a 6.5:1 conical nozzle with a 31 micron throat. The etch was 370 microns deep with a variation of 8 microns in the feature geometry with depth.

Flow rates for a given nozzle linearly vary with chamber pressure. The comparison of like geometries show a slight variation in flow rate as indicated in Figure 9. These are identical samples from different

locations on the wafer. This is most likely due to the variation in channel depth from one sample to the next. The multiplex ICP offers good control of feature dimensions near the surface of the wafer, but as mentioned before, the geometry varies as the etch proceeds. There is also a variation of the etch rate across the wafer, resulting in a distribution of depths for samples. An interferometer measurement can accurately measure depth to about 1 micron, but it is difficult to make the measurements in the narrow throat regions. Thus, an uncertainty of about 10 microns exists in total channel height at the throat.

The nozzle flow rates in Figure 9 are also compared with inviscid theory and the numerical viscous model discussed earlier. As the pressure drop decreases and lower Reynolds numbers are achieved, the flowrate should diverge from the inviscid theory as predicted by the model. However, as is seen by the data points the opposite appears to be true. It appears that the coefficient of discharge is decreasing with increasing Reynolds number. This counter-intuitive result is probably due to the uncertainty in the calibration data supplied by the manufacturer. The error bars displayed on this plot represent the manufacturer supplied tolerances on the calibration data. The linearity and repeatability of data suggests that calibration against known flow rates will allow the proper interpretation of these results.

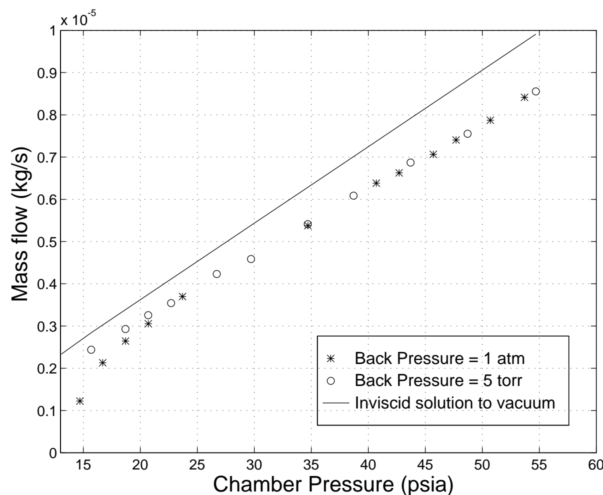

Figure 10: Flow rates in a 7:1 Trumpet Nozzle (throat diameter =31 microns) with varying backpressure.

Figure 10 depicts the variation of flow rate with chamber pressure for a trumpet nozzle exhausting to atmosphere and to a chamber at 5 torr. As the pressure ratio is lowered, the flow rate for two cases remains nearly identical until a pressure ratio of 1.6. This deviation is caused by the flow going subsonic. Thus, this test verifies the existence of a choked condition .

Figure 11 compares the flow rates for three different conical and trumpet nozzles, as well as one bell nozzle which have similar throat diameters and expansion ratios. The similarity in these results indicate that consistent measurements are being made, but the variations in the sample throat diameters and mass flow makes a definitive comparison between different nozzle geometries difficult. A characterization of the variation of coefficient of discharge with nozzle geometry is not offered here due to the uncertainty in the flow meter calibration.

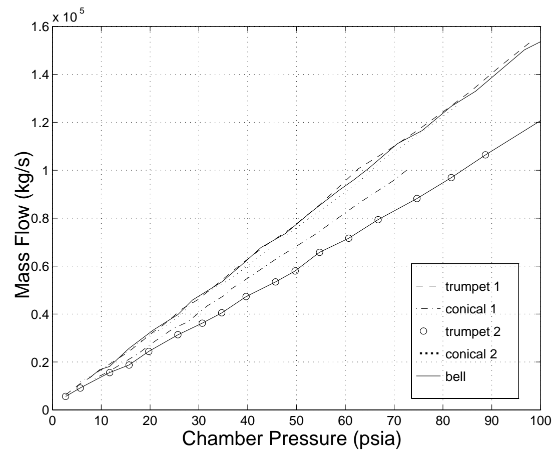

Figure 11: Nozzle flow rates for varying geometries exhausting to an exit chamber of 5 torr. Throat diameters range from 30 - 31 microns.

Conclusions

Sonic nozzle flow can be achieved in micron scale contoured devices to be used in micropropulsion systems. The flow discharge of these devices can be measured, and produce similar repeatable results for similar geometries. Variation in the nozzle flow rates with geometry can be attributed to the uncertainty in the variation in geometry with depth for different samples. Techniques suggested here for maintaining anisotropy during the etch can be performed to obtain a nearly 2-D channel mounted between two parallel glass plates. With a known geometry conclusions about the variability of the coefficient of discharge with geometry can be offered.

Acknowledgments

We would like to thank Dr. Martin A. Schmidt for his insight and advice. This work was supported by the Jet

Propulsion Laboratory with Dr. William Tang as the contract monitor. Additional support was provided from the Goddard Space Flight Center Office of University Programs under the advisement of Dennis Asato.

References

[1] Janson, S. W. "The On-Orbit Role of Electric Propulsion," AIAA Paper 93-2220, June 1993.

[2] Sutton, G. P. *Rocket Propulsion Elements*, Sixth Edition, John Wiley and Sons, New York, 1992.

[3] London, A. P., "A Systems Study of Propulsion Technologies for Orbit and Attitude Control of Microspacecraft", MIT, Master's Thesis, 1996.

[4] Rothe, D. E., "Electron-Beam Studies of Viscous Flow in Supersonic Nozzles," *AIAA Journal*, Vol. 9, No. 5, 1971, pp .804-811.

[5] Grisnik, S.P., Smith, T.A., Salz, L.E., "Experimental Study of Low Reynolds Number Nozzles," AIAA Paper 87-0092, May 1987.

[6] Janson, S. W., and Helvajian, H., "Batch-Fabricated Microthrusters: Initial Results", AIAA Paper 96-2988, July 1996.

[7] Williams, J.C., "Viscous Compressible and Incompressible Flow in Slender Channels," *AIAA Journal*, Vol. No.1, Jan 1963, pp. 186-195.

[8] Rae, W. J., "Some Numerical Results on Viscous Low-Density Nozzle Flows in the Slender-Channel Approximation," *AIAA Journal*, Vol. 9, No. 5, pp. 811-820.

[9] Kim, Suk C., "Calculations of Low-Reynolds Number Resistojet Nozzles," *Journal of Spacecraft and Rockets*, Vol. 31, No. 2, 1994, pp. 259-264.

[10] Zelesnik, D, Micci, M., Long, L., "Direct Simulation Monte Carlo Model of Low Reynolds Number Nozzle Flows," *Journal of Propulsion and Power*, Vol. 10, No. 4, 1994, pp 546-553.

[11] Rohsenow, W. M., and Choi, Harry, *Heat, Mass, and Momentum Transfer*, Prentice-Hall, Inc., Englewood Cliffs, New Jersey, 1961, pp. 284-288.

[12] Arkilic, E. B. "Measurement of the Mass Flow and Tangential Momentum Accommodation Coefficient in Silicon Micromachined Channels", MIT, Ph.D. Thesis, 1997.

[13] Oehrlein, G. S., Rembetski, J.F., and Payne, E.H., "Study of sidewall passivation and microscopic silicon roughness phenomena in chlorine-based reactive ion etching of silicon trenches" *Journal of Vacuum Science Technology*, Vol 8. No. 6., November 1990, p 1199-1211.

[14] Bosch, R., "Method for anisotropically etching silicon", US Patents 4855017, 4789720, Germany Patent 4241045C1.

[15] Wallis, G. and Pomerantz, D. I. "Field Assisted Glass-Metal Sealing: *Journal of Applied Physics*, Vol 40, No. 10 , September 1969 pp. 3946-3949.